Modeling and analysis of rooftop solar potential in highland and lowland territories: Impact of mountainous topography

Apolline Ferry, Martin Thebault, Boris Nérot, Lamia Berrah, Christophe Ménézo

Solar Energy 275 (2024) 112632

Contents lists available at ScienceDirect

Solar Energy

journal homepage: www.elsevier.com/locate/solener

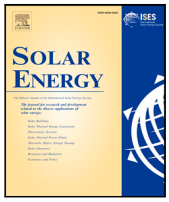

Modeling and analysis of rooftop solar potential in highland and lowland territories: Impact of mountainous topography

Apolline Ferry [a,*], Martin Thebault [a], Boris Nérot [a], Lamia Berrah [b], Christophe Ménézo [a]

[a] University Savoie Mont-Blanc, LOCIE UMR CNRS 5271, Le Bourget-du-Lac cedex, F- 73376, France
[b] University Savoie Mont-Blanc, LISTIC, Annecy-le-Vieux cedex, F- 74944, France

ARTICLE INFO

Dataset link: https://github.com/locie/toscana.git

Keywords:
Rooftop solar radiation
Solar radiation modeling
Solar cadastre
Mountainous territory
Topography
GIS

ABSTRACT

The spatial quantification of solar resources is necessary for the deployment of solar systems and must consider the local specificities of territories, such as complex topography in mountainous areas. This paper presents a methodology for obtaining solar cadastres, based on the Solar Energy on Building Envelopes (SEBE) model incorporated in QGIS and applied to French municipalities. The differences in solar potential between plain and mountain villages are analyzed through the simulation of 92 carefully selected villages located in these two types of regions. The distributions of annual rooftop irradiation per building are obtained for each studied village and approximated with a Johnson's SU density function. From this arises the definition of two statistical indicators: the mode and the spread at one-third maximum. Main results include a mean decrease in the mode of 189 kWh/m^2 and a higher dispersion of 69 kWh/m^2 between mountain and plain villages. Two physical indicators, the Sky View Index (*SVI*) and the Diffuse Fraction Index (*DFI*), are defined to explain these differences in the shape of the distributions. Higher cloud covers (high *DFI*) and the presence of distant shading effects (low *SVI*), caused by terrain relief, explains respectively the smaller modes and the higher dispersion observed in mountainous areas. *SVI*, *DFI* and latitude are fed to a multiple linear regression model, allowing the estimation of distributions with smaller computational costs than the developed methodology. Overall, this analysis demonstrates that the characteristics of mountainous environments greatly influence solar resources and should be considered in energy planning.

1. Introduction

The increasing concerns about the consequences of energy production and natural resources management in the climate change context have led to the development of national and global policies. These policies are essentially oriented towards the reduction of CO_2 emissions over the coming decades by transitioning from conventional to renewable energy sources. In March 2023, the European Union revised its renewable energy targets, aiming to achieve a 42.5% share of renewables by 2030 in line with the objective of attaining carbon neutrality by 2050. To expedite progress toward these renewable energy goals, a law called 'Accelerating Renewable Production' was enacted in France in March 2023 [1]. This law empowers local authorities to identify areas with high renewable energy potential within their territories, underscoring the need to assess potential at the local level.

All territories must be considered, and among them, mountain regions, which were often overlooked in energy policies until recently [2,3], despite their importance being acknowledged as early as 1992 during the United Nations Conference on Environment and Development [4]. The mountain territories represent 25% of the world's land area and 12% of the population [5] : they require sustainable development and protection. Furthermore, these areas possess substantial renewable energy resources, including wind energy (high wind speed) [6], hydroelectricity (headwaters located in mountains) [7] and biomass (one third of forests located in mountains) [8]. Solar energy also holds potential, considering both photovoltaic, with reduced loss factors due to low temperatures, and thermal systems [9]. This energy production can address the high residential energy demand in these regions, particularly in winter [3,10], driven by harsh climatic conditions and in some cases an aging building stock with poor thermal properties [9]. It can also enhance their energy independence, a necessity due to their remote locations [3], thus reducing energy transport losses, and increase economic and social development for lower population density region [11]. Currently, economy of mountain region heavily relies on ski tourism, which is significantly impacted by climate change and energy resources. Rising temperatures make them vulnerable to snow scarcity. Snow supply risk can be mitigated through snowmaking but requires substantial resources in terms of electricity

* Corresponding author.
E-mail address: apolline.ferry@univ-smb.fr (A. Ferry).

https://doi.org/10.1016/j.solener.2024.112632
Received 16 November 2023; Received in revised form 20 February 2024; Accepted 16 May 2024

and water [12]. Thus, mountainous regions are undergoing changes on both socio-economic fronts, with a mandatory transformation of their activities, and on the energy front, as there is a growing need to develop renewable energy sources. Therefore, new smart approaches have been tested recently to implement sustainable strategies in ski resorts and maintaining sustainable winter tourism [2].

Among all renewable resources, solar energy is one of the most promising sources of energy, with the sun being a clean and abundant source across the entire surface of the globe. Technological progress, decreasing costs and increasing public acceptance, even in alpine regions [10], have led to a growing share of solar energy in the world energy mix. To ascertain the potential development of solar systems, especially within the build environment, precise and accurate modeling of solar irradiation is needed. Solar cadastres quantify solar irradiation through a mapping of its spatial distribution [13]. Geographical Information System (GIS) tools facilitated their development in recent years [14], in particular regarding urban areas [15,16] or for country-scale studies [17,18]. Conversely, there have been very few cadastres addressing mountainous regions [19,20], despite their differences from urban areas.

Indeed, the causes of solar resources variations are two-folds. On a global scale, the variations come from latitudinal gradients caused by the Earth's geometry and its rotation and revolution around the sun. At regional and local scale, topography is the primary factor influencing the radiation distribution, with variations in elevation, slopes, and surface orientations [21]. Topography affects all three components of global solar radiation [22]:

- Direct normal radiation is influenced both by variations in the angle of incidence due to surface orientation and slope, as well as by the surrounding topography, which can obstruct the direct sun beams [22].
- Diffused radiation is reduced by mountains because there is a smaller proportion of visible sky [23,24].
- Reflected radiation is more pronounced in mountainous areas compared to plains due to the increased number of surrounding surfaces that can reflect radiation [25].

Three topographic components have been identified by Olson and Rupper [26]: cast shadows from the surrounding topography (blocking the radiation), shaded terrain or self-shadowing by the slope itself (occurring when the incident angle is greater than 90°), and the aspect and slope (altering the incident angle). The impact of these three effects have been assessed individually and it has been demonstrated that each component can be predominant depending on the surface's location [26]. The estimation of shadow is an essential part of solar resource assessment as shadow could have negative impact on solar systems, especially photovoltaic, due to possible mismatch losses [27].

The estimation of solar resources is highly challenging in mountainous areas, with significant inaccuracies in the radiation values estimated using conventional methodologies compared to plain regions [28]. Consequently, several approaches have been developed for generating solar radiation maps on complex terrain [29–31]. The first GIS-based radiation models were developed at the end of the 20th century based on empirical formulas that allowed the spatial mapping of solar radiation, taking into account slope inclination, aspect, and shadowing effects based on Digital Elevation Model (DEM). Notable examples include *SolarFlux* [24,32], a series of solar radiation algorithms in *Genasys GIS* [33], *Solei* in the *IDRISI GIS* software [34,35], and *SRAD* [36]. More advanced algorithms have subsequently been developed, such as *Solar Analyst* developed in *ArcView GIS*, which generates upward-looking viewsheds to consider sky obstructions [37], or *r.sun*, which is suitable for large areas [21]. The significance of having a high-resolution DEM to account for shading phenomena in mountainous regions has been demonstrated in comparative studies with experimental data [22,38].

New and diverse approaches have subsequently emerged to consider topography, and improve the precision of results, the size of the studied regions, or calculation speed. López et al. introduced a parametric model to derive daily values of clear-sky global solar irradiation based on various parameters, considering the horizon obstruction by calculating synthetic irradiation using the *SMARTS* algorithm [39,40]. Satellite imagery (*Meteosat*) has also been employed by Bosch et al. [41] in combination with a Digital Terrain Model (DTM) and the *Heliosat-2* algorithm, with a new horizon calculation method to reduce computational costs. An empirical approach coupled with kriging interpolation was employed by Park et al. [42] to produce an irradiation map for South Korea, incorporating a topographic factor to address the complex terrain. However, spatial interpolation can be challenging for studies at smaller scales in mountainous areas, as the number of measurement stations is limited. Consequently, the use of deep learning, like neural networks, has also been tested [43–45].

The previous studies primarily focus on estimating solar resources over large territories but provide limited insight into the amount of energy received by buildings. Some studies have been conducted at the village level, with a particular focus on two villages in the mid and high mountain regions. The first village, Hemberg, located in Switzerland, is situated at 954 m and comprises 154 buildings [46,47]. The renewable potential of the village was assessed using radiation data from a previous study [48] and a combination of software tools, including QGIS for the creation of the DSM and CitySim for the calculation of photovoltaic potential and energy demand. It has been demonstrated that more than half of total energy demand can be covered in this village by renewable energy sources, including PV and wind turbines, considering some energy renovation scenarios [47]. It has also been shown that it is possible to increase the renewable energy fraction in the future with sustainable scenario of this village thanks to an increasing share of PV panels production in the renewable production [46]. Then, the Swiss village of Zernez, located at an elevation of 1474 m and consisting of 154 buildings, has been the subject of studies [49,50] to examine the rooftop solar potential and optimize the location of photovoltaic installations, as well as explore the synergy with other renewable energy sources. Particular attention was given to considering the terrain's topography using a raster approach, utilizing *ArcGIS* for DSM construction and *ArcMap* for irradiation calculations across the entire surface. These studies at the village scale demonstrate, thanks to the use of solar potential maps, that PV systems can play a major role in the energy transition of these mountainous villages. Finally, the building-scale at high altitude was investigated by Notzon et al. [51], who examined the potential energy generation through photovoltaic systems on buildings located at 2469 m above sea level at the Great St Bernard Pass. The study reveals that the presence of snow on the ground and low temperatures lead to higher energy production than in lowland regions during the summer. However, the presence of a snow cover significantly diminishes this production during the winter.

Despite the increasing consideration of topography models at a regional scale in mountainous areas, there is a lack of multi-scale studies regarding the irradiation received by buildings spread across an entire mountainous massif. Furthermore, to the best of our knowledge, there are no studies comparing solar potential between mountainous and plain areas at the village-scale.

The main contributions of the present paper are thus:

- The development of a methodology to obtain solar cadastres, based on open-access databases, specially suited for large-scale mountainous territories;
- The implementation of a statistical approach, applied on more than 90 municipalities (representing 3627 km^2 in total), enabling the comparison of rooftop irradiation distributions in mountainous and lowland villages;
- The analysis and the identification of easily computable weather and topographical factors explaining differences in distributions of irradiation within the studied villages;

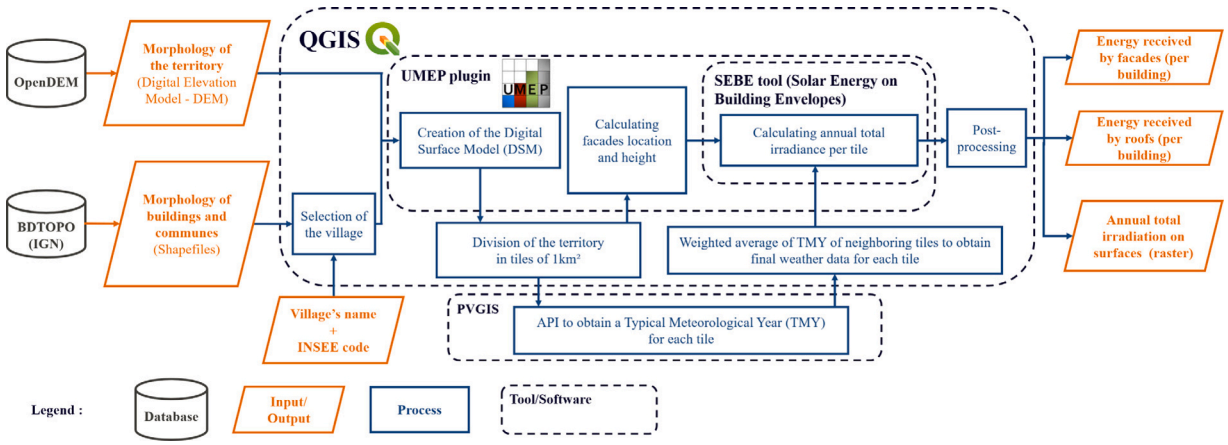

Fig. 1. Workflow of the developed methodology to obtain solar cadastres and to model annual cumulative irradiation received by buildings roofs and facades.

- The prediction of the statistical rooftop irradiation distributions through a limited set of morphological and meteorological indicators;
- The establishment of recommendations on how these results could help the energy transition planning in mountainous villages.

The remainder of the paper is organized as follows. Section 2 outlines the developed methodology. It consists in an adaptation of existing tools for modeling solar irradiation, to the specific case of large-scale mountainous territories. Section 3 describes the villages selected as case studies and the selection process. Section 4 presents the distributions of rooftop irradiation obtained for the cases studied. These are fitted to an analytical function and characterized with carefully selected indicators. The differences between lowland and highland villages are consequently described through morphological and meteorological indicators, and the predictions of the distributions are done through multiple linear regression of these indicators. Finally, Section 5 presents the impacts on energy transition planning, future developments of this study and some uncertainties and limitations of this work.

2. Methodology

2.1. General framework

In this section, the methodology developed (see Fig. 1) to determine solar potential in both mountainous territories and lowland areas is presented. It relies on open-source tools and open-access databases as input [52], offering the possibility to reproduce the results and simulate large territories. Its main output is a solar cadastre, also called solar map, which is a large-scale mapping of the solar potential [15].

The developed approach is based on the GIS software *QGIS*, which is free and open-source. *QGIS* was chosen due to its *Python* extension, which enables process automation and acceleration.

The methodology begins with the use of two databases covering French territory (see Section 2.2).

First, a French municipality is selected based on an unique code attributed by the French National Institute of Statistics and Economic Studies (INSEE [53]). Buildings data and the DTM corresponding to municipal territory of this village are collected.

To enable the inclusion of building heights in the Digital Terrain Model (DTM) and thereby to generate a Digital Surface Model (DSM), a spatial resolution of 1 meter is required. In order to attain this resolution, the DTM is resampled using a bilinear method (*Warp Reproject* function from *GDAL* library, allowing for reading and writing raster and vector geospatial data formats, used in *QGIS* [54]). This would not have been possible with the initial coarse resolution of 25 m. The pixels' elevation is then modified according to the buildings' height to create the DSM (see Section 2.2).

The next step is the division of the territory into tiles in order to account for the heterogeneity of the mountainous territories and for computational purpose as described in Section 2.3. For each tile, meteorological data files are obtained through an Application Programming Interface (API) from the *PVGIS* tool [55]. The meteorological files employed are Typical Meteorological Year (TMY) files, providing representative values over 15 years. The most recent period (2005–2020) has been chosen. The final weather file used for each tile is a weighted average of several weather files from neighboring tiles, allowing for consideration of the lower spatial resolution of the weather files than the tile size (see Section 2.3).

The calculation of building facade orientations and heights is then carried out with the *Wall Height and Aspect* function from *UMEP*. Subsequently, the calculation of irradiation is performed using the SEBE tool (Solar Energy on Building Envelopes) for each tile [56], as presented in Section 2.4. This tool generates an irradiation map on the surfaces of the territory of the considered tile. The results from the different tiles are gathered in one file using the *Merge* function from *GDAL*.

The roof irradiation is then obtained by superimposing the irradiation map and building footprints. Finally, for each roof, the calculated cumulative annual irradiation is then spatially averaged using the *Zonal Statistics* tool from *QGIS*, so that each roof is associated with a single value, representing its spatially-averaged cumulative irradiation. A buffer of 1.5 m was previously applied, using the *Buffer* function from *QGIS*, to reduce the building footprints. It was done in order to prevent inconsistencies related to building's edges effects caused by the pixel resolution of the irradiation map.

2.2. Databases

The selection of suitable databases was challenging as they needed to be uniformly accessible in the same standardized format across all the territories under investigation, in order to ensure the consistency and comparability of the different simulations.

2.2.1. Geographical databases

Two sets of geographical data are required:

- A DSM and eventually a DTM, which are raster layers containing elevation values. It is particularly needed in mountainous area to consider the surrounding topography. A DSM differs from the DTM by containing also the elevation of buildings and sometimes vegetation. A DTM is only required to build the DSM if the DSM is not directly available.

- Building geometry vector layers, with a morphological description of buildings. Footprints and heights of buildings are necessary to have a 3D representation of structures.

The used database are :

- The *EU-DEM* model [57], which has been developed thanks to Copernicus, the European Union's Earth observation program. This digital model covers 39 countries of the European Environment Agency. The spatial resolution of this DTM is 25 m.
- The *BDTOPO* database [58], a 3D vectorial description of elements of the French territory produced by the French National Institute of Geographic and Forest Information (IGN). The objects contained in that database are gathered by themes: *Administratives* and *Built* are used in this work to obtain boundaries of municipal territories and building footprints and information.

DSM were not available in open-access for the French territories, they were therefore built using the *DSM Generator* function from *UMEP*, by superimposing the DTM and the building geometry layer and adding the specific height of each building to the ground elevation values corresponding to the building footprint location. It is important to note that this function assigns a unique height to the entire building footprint, resulting in flat rooftops. The currently available data do not allow us to know the actual orientation and slope of each roof section for such a large amount of buildings and municipalities. It was thus decided to work with flat roofs since it provides homogeneous data for all considered buildings and valuable insights of incoming irradiation at roofs level.

The use of alternative databases, in order for example to apply the methodology to another country, is of course possible, but could required preprocessing steps.

2.2.2. Meteorological databases

Irradiation databases constitute the second type of databases required for this study. The solar radiation database PVGIS-SARAH2, derived from the second version of the Surface Solar Radiation Data Set - Heliosat (SARAH-2) was chosen for investigation. The dataset is accessible in PVGIS, where an API is available and facilitates data retrieval [59]. This dataset is derived from satellite observations of the geostationary Meteosat satellite and has been validated with ground measurement [60]. Satellite data enable the utilization of long-term average time series and coverage over a large geographical area. This database covers Europe, as well as some parts of South America, Asia, and Africa. The spatial resolution of SARAH-2 dataset is 5 km, but the irradiation data are refined by PVGIS at a smaller spatial scale considering the mask through a DTM with a resolution of 3 arc-seconds. It allows for horizon calculation and determines when the sun is behind mountains. During these times, solar irradiation originates solely from the diffuse component of radiation. A TMY weather file generated by PVGIS has been chosen for the study with a temporal resolution of 1 h.

2.3. Tiling methodology

Tiling is an important part of the methodology. Indeed, tiling has been set up in order to consider the spatial variation of the terrain. The meteorological files from *PVGIS* take into account distant masks. Using a single weather file for the entire territory would work well for lowland areas, without any strong elevation variations within the municipality and around it, where irradiation distribution is relatively uniform. However, this would not be the case for the mountain villages, where the presence of complex terrain induces a high variability in elevation, slope, and orientation of surfaces, thereby modifying the spatial distribution of solar radiation. Therefore, using tiles allows to have different meteorological files for one village.

It is also necessary given the large areas of the investigated territories that have been processed with the SEBE tool. Some calculation steps are computationally intensive, and dividing the territory into tiles helps to reduce the processing time.

To set up the tiling, a 1 km × 1 km grid was created using *Create grid* function from *QGIS*. Each grid tile was then used to clip the data using *Clip raster by mask layer* function from *GDAL*. Weather data are obtained through the PVGIS API for each center of tile.

However, due to the low resolution of SARAH-2 database, significant variations in the meteorological data may be observed between two adjacent 1 km simulation tiles if they are associated to two distinct 5 km weather tiles. A weighted average of the meteorological data from the studied tile and its 12 nearest neighboring tiles has been computed to reduce these variations. The weighting coefficients were determined according to the normal distribution based on the normalized distance from the center of the tile (Eq. (1)). This method effectively smoothed out the resolution disparity between meteorological data and the chosen tile size for simulation, while accounting for masks and large territorial areas.

$$c(i) = \frac{f\left(\frac{x(i)}{\max(x(i))}\right)}{\sum_{i=0}^{12} f\left(\frac{x(i)}{\max(x(i))}\right)} \tag{1}$$

with f the standard normal distribution, x the distance to the center of the studied tile, and i the different neighboring tile, with $i = 0$ being the studied tile.

2.4. Description of SEBE tool

SEBE tool has been used for this study as it is integrated in QGIS and both are open source. SEBE has been developed by Lindberg et al. [56] and allows to estimate shortwave irradiation, on the ground, rooftops and facades of buildings. This tool has been validated against on-site measurements and shows a good performance for roof and facades irradiation evaluation [56]. SEBE tool is classified as a 2.5D model, using DSM and DTM in raster format (2D) to get irradiation information on the geometry surfaces, with irradiation values available on the ground plane and along the facade height. The use of raster for terrain morphology (DSM and DTM) allows implementation over large areas, as the time required for calculations is reduced compared to a vector-based methodology [56]. To have an accurate estimation of the solar irradiation, shadow patterns from buildings and ground topography need to be considered. SEBE use a "shadow volumes" methodology that have been developed by Ratti and Richens [61]. This methodology allows to determine, for each azimuth and altitude angle of the sun, whether surfaces are in sunlight or shade.

The other input of the SEBE tool, apart from terrain description, is meteorological data. The model needs direct, diffuse and global irradiance. If the diffuse irradiance is not available, this component could be estimated from the global irradiance thanks to Reindl et al. method [62], and the estimation could be improved with ambient air temperature and relative humidity data. In this study, diffuse and direct components have been estimated from weighted average of global irradiance, temperature and relative humidity.

For each simulation, the diffuse and direct components are redistributed into patches of similar solid angles throughout the sky vault and then summed over the investigated period, in order to follow the approach developed by Tregenza and Sharples [63]. Thus, SEBE produces annual cumulative irradiation map.

The Plane of Array (POA) irradiance is thus calculated as the sum of direct, diffuse and reflected components of the irradiance for each patch of the sky vault decomposition, while considering the shadows cast by buildings (Eq. (2)) [56]. In the present case, the vegetation was not considered for the shadow calculation since suitable databases were not available. The POA Irradiation received over an entire year will be referred to as annual cumulative irradiation throughout the remainder

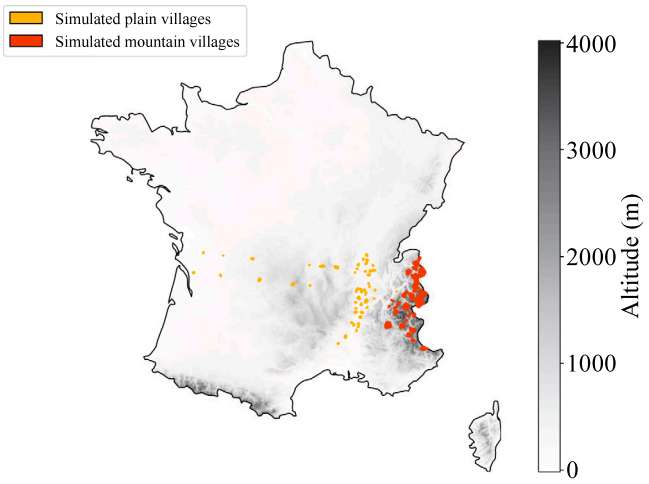

Fig. 2. Topographic map of France with the simulated villages. The gray color scheme indicates the elevation. Mountain villages are represented in red and plain villages in orange. Villages at iso-latitude than Tignes and Le Grand-Bornand (mountainous villages) can be seen on the west of the map. (For interpretation of the references to color in this figure legend, the reader is referred to the web version of this article.)

of the study, in accordance with the annual cumulative irradiation map generated by SEBE.

$$POA = \sum_{i=1}^{p} [(DNI \cdot \omega \cdot S + DHI \cdot S + GHI(1 - S)\alpha)]_i \quad (2)$$

where p represents the number of patches of the hemisphere, DNI the incident direct radiation, DHI the diffuse radiation, GHI the global radiation from the ith patch, α the surface albedo, ω the sun incidence angle and S the shadows from buildings (and optionally from vegetation).

In one simulation, a single albedo value can be selected to be applied to all the surfaces and in this work, the albedo was set to $\alpha = 0.15$ for all the simulations, which is a typical value for solar potential simulations [21,64], in a peri-urban environment composed of trees, grass and buildings [65,66]. The same albedo value is assumed for plain and mountainous villages. Note that the presence of snow in mountainous areas significantly increases albedo during winter months but has complex effects, as snow can cover rooftops and solar installations, substantially reducing energy production [67]. This phenomenon is intricate and would required in-depth analysis. Since this study focuses mostly on the impact of mountainous topography on irradiation, the impact of snow is disregarded. This point is further discussed in Section 5 regarding the limitations and future developments of this study. Due to the nature of the study, which focuses on irradiance on flat rooftops, the impact of albedo change is limited.

3. Presentation of the case studies

In this work, the distribution of the annual irradiation on rooftops of buildings in mountainous municipalities is investigated. To that aim, mountain villages in the French Alps were selected, represented in red in Fig. 2. These villages are distributed across the entire Alpine massif, providing a wide range of locations at varying latitudes. They were specifically chosen as they are all ski resorts, ensuring that the villages share similar characteristics.

Subsequently, each mountain village was paired with a village located at the same latitude but located in a plain area, far from mountainous areas (represented in orange in Fig. 2). In what follows, these villages will be referred to as 'plain villages'. These plain villages do not exhibit significant terrain compared to the ski resorts. These villages are situated in the Rhône valley, which is the closest plain area to the Alps. By pairing each mountainous village with a plain village, it is possible to investigate the distribution of irradiation on rooftops while eliminating the impact of latitude. Indeed, differences in latitudes would imply different sunpaths and, therefore, variations in solar irradiation.

Note that among the plain villages, two sets of municipalities with identical latitudes were also selected, and used in Section 4.6 to assess the variation in irradiation for different longitudes over the French territories.

When selecting the case studies, pairs of villages with similar numbers of buildings were chosen in order to keep consistency when comparing them. Nevertheless, because of the lower density in the Alps, mountainous villages typically have much larger land areas than plain villages with same number of buildings. The average characteristics of the selected villages in mountain and plain have been summarized in the Table 1.

Table 1
Summary of the main characteristics of the studied villages.

Characteristics	Mountain villages	Plain villages
Number of village	38	54
Mean altitude (m)	1918 ± 329	312 ± 164
Number of buildings	1902 ± 1499	1018 ± 907
Municipality area (km^2)	74 ± 69	15 ± 10

4. Results and analysis

First, irradiation maps obtained using the methodology described above are presented. Subsequently, the annual cumulative irradiation received specifically by each building rooftop is obtained in the form of distributions, which are then approximated by a density function. This function allows the establishment of indicators for characterizing the distributions and facilitates the comparison of irradiation distribution profiles between lowland and mountain areas. Two morphological and meteorological indicators are then defined to describe the impact of the mountain environment. Finally, a prediction of irradiation distributions is presented, derived from the previous indicators, along with latitude as a contributing factor.

4.1. Irradiation maps

The developed methodology allows to generate irradiation maps with the annual total irradiation per square meter. Illustrations of these maps, for the villages of Le Grand-Bornand and Trévoux, are presented in Fig. 3. On the magnified view (Fig. 3a), the shape of the buildings can be recognized and shadow zones around the buildings can also be observed. The lack of consideration for roof slopes is also evident, with minimal variation of irradiation in the roof surface of buildings.

The complex terrain is indeed considered in the mountainous village (Fig. 3a), with the appearance of areas that are shaded by mountains, corresponding to north-facing slopes that receive less irradiation than south-facing faces. The low irradiation zones are thus much larger for mountainous regions (Fig. 3a) compared to those in plains (Fig. 3b) with areas of shadow caused by the presence of terrain relief being added to those resulting from buildings' shading. The variation in irradiation within the village's territory is significant and can reach up to 1000 kWh/m^2 between areas on different hillsides.

4.2. Distribution of irradiation on rooftops

The average rooftop irradiation is then calculated for each building. As previously mentioned, the rooftops are modeled as flat because of the lack of roof characteristic data. Thus, it corresponds to an average horizontal rooftop irradiation per building.

The distributions of average annual irradiation per building are plotted as density function in Figs. 4 and 5. The height of each bin

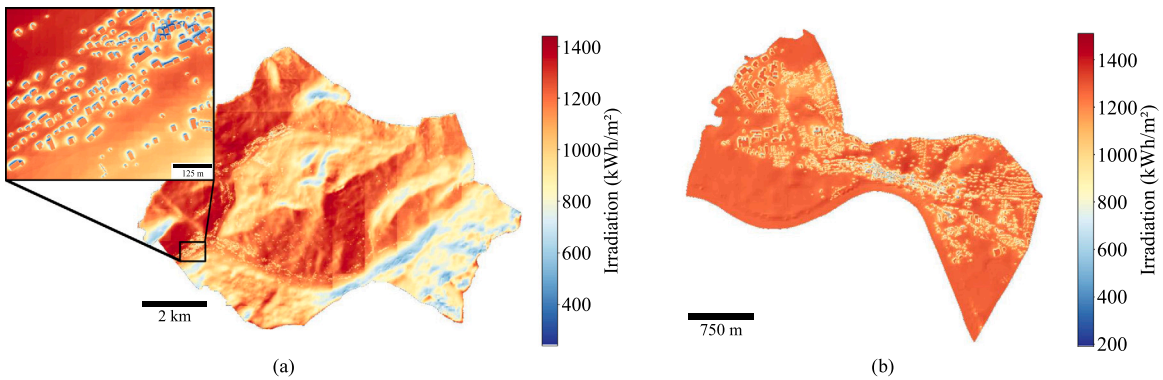

Fig. 3. Illustration of irradiation map (Annual total irradiation in kWh m^{-2}) obtained with the developed methodology (a) for the entire mountain village of Le Grand-Bornand (lat.: 45.942°, long.: 6.427°, alt.: 1527 m) with a magnified view of the center of the village and (b) for the entire plain village of Trévoux (lat.: 45.942°, long.: 4.775°, alt.: 190 m).

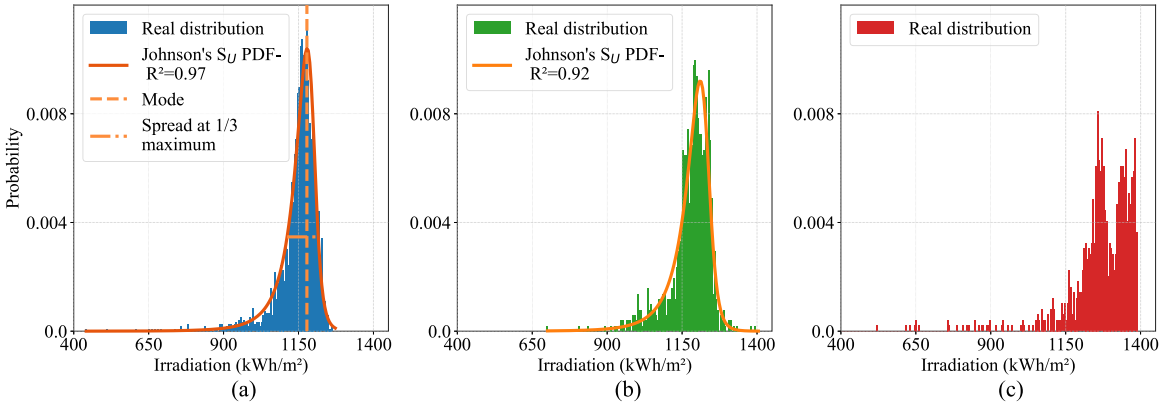

Fig. 4. Distributions of average annual irradiation on building rooftops for three villages: (a) for the northern Alps village of Le Grand-Bornand (lat.: 45.942°, long.: 6.427°, alt.: 1527 m), (b) for the southern Alps village of Vars (lat.: 44.61°, long.: 6.688°, alt.: 2263 m) and (c) for the mountain village of Huez (lat.: 45.081°, long.: 6.052°, alt.: 2032 m). The Johnson's S_U distribution estimation are displayed also for Le Grand-Bornand (a) and Vars (b). For the village of Huez (c), two peaks can be observed, preventing the fitting of Johnson's S_U estimation.

in these figures corresponds to the proportion of buildings of the studied village receiving an average annual rooftop irradiation within the corresponding range.

These distributions were obtained for all the studied municipalities, but present different characteristics if the villages are located in plains or in mountains. The two cases are described in what follows.

4.2.1. Distributions for mountain villages

Two types of distributions are obtained for the mountain villages. For the majority of the villages, the distributions show similar shapes regardless of the village: whether the village is located in the southern Alps (Fig. 4a) or northern Alps (Fig. 4b). In all these distributions, a peak is formed around the mode (the irradiation with the highest probability value) corresponding to the irradiation received by the majority of the buildings in the village.

Few buildings receive significantly higher irradiation, corresponding to buildings with perfect location like a south-facing mountainside. On the other hand, more buildings receive an irradiation that is lower than the peak, forming a long tail of distribution towards low irradiations.

A second type of distributions appears also for some villages: two (and sometimes three) distinct peaks are present (Fig. 4c). It concerns about one fourth of the mountain villages (10 out of 38). A widespread village or a village forming two distinct zones, with for example the center of the village in the valley and a hamlet at higher altitude, can create these types of distributions. If these distinct areas are located on different mountainsides or at different altitudes, irradiation range could be very different. Thus, mountain villages could be constituted of "irradiation sub-villages", with for each of these "sub-villages" a distribution that is similar to the distribution of the other mountain villages.

The width of the peak varies depending on the location of the village, with larger peak width for mountain villages. The tails of the distribution is also larger for these mountain villages with more buildings receiving less irradiation than the peak in mountains compared to plains. This difference is explained by the presence of terrain. Indeed, topography can, on one hand, result in buildings in mountain villages being situated on different mountainsides, causing some buildings to suffer from shadowing on the north-facing sides. Additionally, terrain also acts as a distant mask, blocking solar radiation during certain parts of the day, thereby reducing the amount received by specific buildings. Hence, these two effects combine with the overshadowing phenomenon due to surrounding buildings, which is also present in mountainous areas. This results in a higher variability and lower values of average rooftop irradiation among buildings within the municipal territory in mountainous regions.

4.2.2. Distributions for plain villages

The shape of plain village distributions is broadly similar to those of mountain villages (Fig. 5a), with the appearance of a peak. However, unlike mountain villages, the emergence of several peaks (due to several zones) is very rare. Indeed, plain villages are much less extensive than mountain villages (Table 1) with the majority of buildings located within the same area. In plains, the tail of the distribution corresponds almost exclusively to buildings that are overshadowed by others, as variations in elevation are very slight. Thus, an overwhelming majority

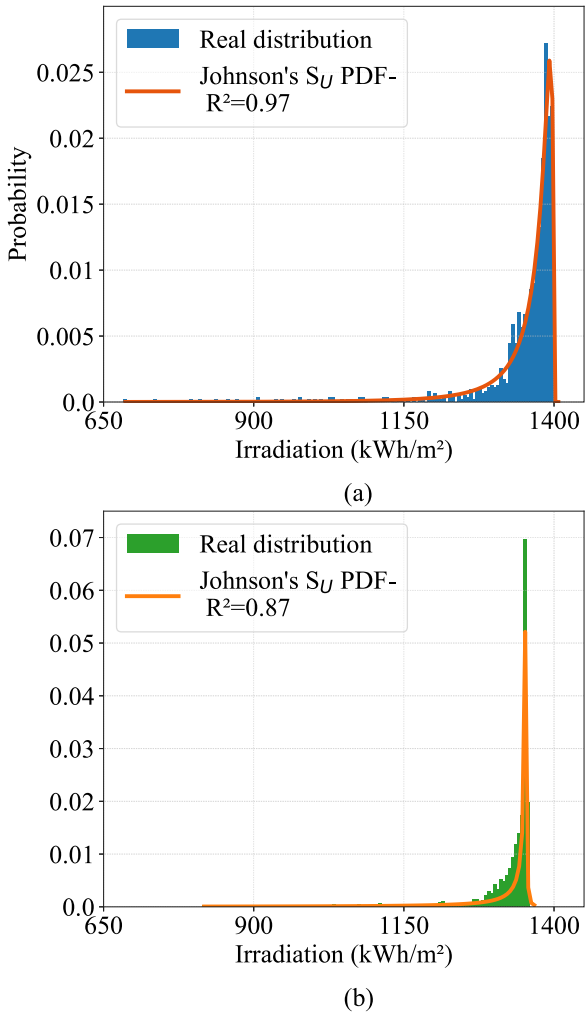

Fig. 5. Distributions of average annual irradiation on building rooftops and their Johnson's S U distribution estimation for the lowland villages of (a) Leyment (lat.: 45.922°, long.: 5.298°, alt.: 247 m) and (b) Reventin-Vaugris (lat.: 45.468°, long.: 4.841°, alt.: 270 m).

of buildings will receive a rooftop irradiation in a very narrow range of values, which can create very high peaks in the distributions (Fig. 5b).

4.3. Approximation by Johnson's S_U function

Since a large majority of distributions exhibit a similar shape, an analytical approximation function was looked for in order to represent the data distributions. It appeared that Johnson's S_U function could fit well the distributions. Note that all the distributions from the *scipy.stats* python module [68] were tried out but Johnson's S_U function provided the best fit. The Johnson's S_U "unbounded system" distribution is a four-parameters probability density function (Eq. (3)) that could be expressed as a transformation of the normal distribution (Eq. (4)) [69]. The Maximum Likelihood Estimation method was used to fit the function to the observations and allows the estimation of fitting parameters a, b, c, d.

$$f(x,a,b,c,d) = \frac{b}{d\sqrt{2\pi}\sqrt{1+\left(\frac{x-c}{d}\right)^2}} \times \exp\left(-\frac{1}{2}\left(a + b\,\mathrm{arcsinh}\left(\frac{x-c}{d}\right)\right)^2\right) \quad (3)$$

$$f(y,a,b) = \frac{b}{\sqrt{y^2+1}}\phi\left(a + b\log\left(y+\sqrt{y^2+1}\right)\right) \quad (4)$$

with ϕ the probability density function (PDF) of the normal distribution and $y = \frac{x-c}{d}$.

x, a, b, c, d are reals, c is the location parameter and d is the scale parameter.

The superimposition of the raw data distribution and the Johnson's S_U function in Figs. 4 and 5 demonstrates that this approximation provides a good fit of the data distribution. The fitting holds true for mountain villages with one peak in the distribution but also for almost all plain villages, regardless of their typology and location.

In order to assess the fitting quality of this approximation function for the studied villages, the coefficient of determination, denoted by R^2, was calculated. This metric indicates the goodness of the fit between the Johnson's S_U approximation to the raw data distributions and is defined in Eq. (5).

$$R^2 = 1 - \frac{\sum_{i=1}^{b}(y_i - \hat{y}_i)^2}{\sum_{i=1}^{b}(y_i - \bar{y})^2} \quad (5)$$

with :

- b : Number of bins in the distribution, set to 150 for all the villages, which corresponds to the number of observations
- y_i : Observed values of probability for data point i
- $\hat{y}_i$: Predicted values of probability with Johnson's S_U approximation for data point i
- $\bar{y}$: Mean of observed values of probability

R^2, was calculated for each distribution and have been displayed on Figs. 4 and 5. Regarding plain villages and mountain villages with one peak, R^2 ranges from 0.46 to 0.99 with an average value of 0.86 and standard deviation 0.11. These high values show the high suitability of Johnson's S_U distribution to describe the observed distributions, in particular for mountain villages where average R^2 is 0.94.

Using a analytical PDF function, instead of a discrete probability distribution, has the advantage of being able to obtain the probability associated with each irradiation value, as well as accessing certain properties of the distribution through its analytical expression. This also enables easier characterization of the distribution and facilitates its representation and reproduction.

Since more than 90 municipalities are considered here, a simplified description of distributions and their respective Johnson's S_U approximations is needed. Therefore, for the sake of clarity, two statistical indicators were defined to characterize the distributions:

- The *Johnson's S_U mode*, which corresponds to the irradiation value with the highest probability.
- The *peak width* or *spread at one-third maximum*, which have been obtained by calculating the difference between the two irradiation values that have a probability equal to one-third of the mode's probability.

These two indicators allows to simply characterize the distribution of irradiation for each village. They have been reported on Fig. 4a.

4.4. Clustering in mountainous villages

Presence of complex terrain could induce the appearance of several peaks in the annual rooftop irradiation distribution of certain villages as illustrated in Section 4.2.1. Therefore, it is not possible to fit the Johnson's S_U distribution to the distribution of these villages but could be possible for each peak separately as their shapes are similar to the shape of the distribution of the other villages. In order to understand and explain the presence of several peaks, buildings were split into groups using a clustering algorithm. The K-medoids algorithm partitions the data in groups by minimizing the distance between points of a same group and select actual data points as centers of the cluster, called medoids. This algorithm [70], available in the *scikit-learn-extra* library, was chosen as it is robust to outliers. For each building, normalized

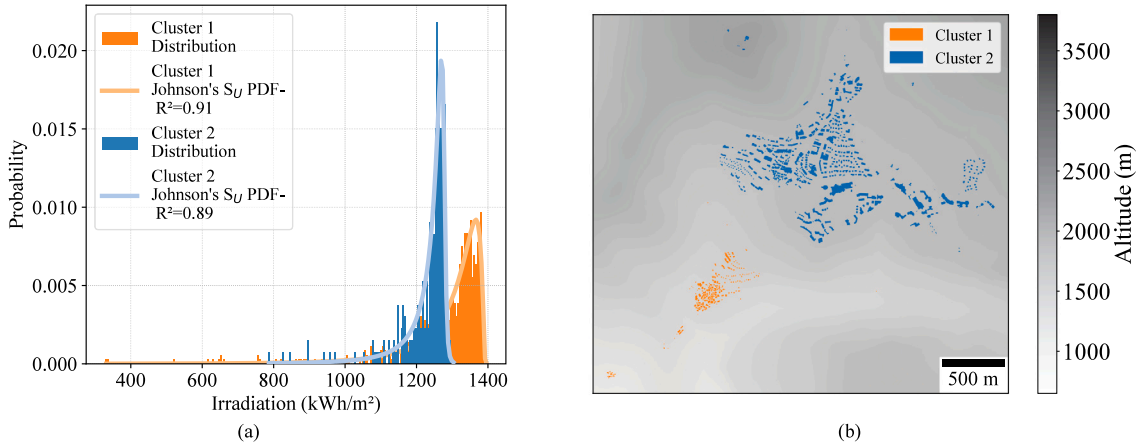

Fig. 6. (a) Distributions of average annual irradiation on building rooftops and their Johnson's S_U distribution estimation for the two buildings clusters for the mountain village of Huez (lat.: 45.081°, long.: 6.052°, alt.: 2032 m) and (b) topographic map of the center of the village of Huez with the location of the two clusters. (For interpretation of the references to color in this figure legend, the reader is referred to the web version of this article.)

values of latitude, longitude and altitude were obtained. They were used as input data of the clustering algorithm to divide buildings into groups as illustrated in Fig. 6b. The number of clusters was selected accordingly to the number of peaks observed in the distributions. The clustering algorithm allows to identify groups of buildings that are present in the villages. These groups can come from the large extent of territories with buildings located in different valleys or can be form by the morphology of the territory with groups located on different mountainsides or at different altitudes.

Then, distributions of rooftop irradiation were obtained for each cluster and were fitted to the Johnson's S_U distribution 6a. Clustering effectively divide the distribution according to the different observed peaks with a fit of the Johnson's S_U function as good as for other mountain villages. Thus, the topography and the morphology of territories can explain that groups of buildings could receive different quantities of irradiation.

Among the ten studied villages that have several peaks, clustering allows to obtain two Johnson's S_U distribution for seven of them with an average R^2 of 0.90. For the three remaining villages, clustering does not however allow to explain the complexity of these mountain villages.

The two indicators described in Section 4.3 can be calculated to characterize the "sub-villages", which will be used in the rest of the study.

4.5. Comparison between mountain and lowland villages profiles

The generation of distributions of average annual irradiation on building rooftops and Johnson's S_U distribution estimations for all the case studies enables comparisons between lowland and mountain villages, particularly for pairs of villages at the same latitude. For each pair of mountain/lowland villages, the distribution of the mountain village is shifted towards low irradiation compared to the lowland village as shown on Fig. 7. This shift is systematic, but its magnitude varies depending on the characteristics of the two villages. The average shift of the mode between plain and mountain villages is around 189 kWh/m^2 for all the investigated pairs.

The shape of the peak differs between the two village typologies, with a greater peak width for mountain villages and a sharp peak for lowland villages. Indeed, the average value for the spread at one-third maximum is 108 kWh/m^2 for mountain villages while being only 39 kWh/m^2. Thus, the spread of the distribution of the average annual irradiation on buildings increases with the presence of topography.

The mode values and the spread at one-third maximum have been plotted against the latitude for all the considered villages (Fig. 8). Two clear trends can be observed. First, the mode decreases with the latitude (Fig. 8a). This is expected since as latitude increases, in the northern hemisphere, the irradiation received on flat surfaces globally decreases [71]. Latitude does not significantly influence the spread, as the dispersion of irradiation values is mainly due to local spatial variation in buildings and terrain (Fig. 8b). But most importantly, it is clearly possible to see the difference between mountain and plain villages for each latitude on both figures, with lower modes and higher spreads at one-third maximum in the mountains than in the plains.

Consequently, these two figures show that the two indicators employed to describe the distributions allow to separate mountainous villages from those in lowlands and can be used to differentiate them.

4.6. Influence of the mountainous terrain compared to the longitude variability

In order to assess whether this shift in the irradiation distribution is also impacted by the longitude over the French territories, the irradiation distribution of two mountainous villages, Tignes and Le Grand-Bornand, have been plotted (see Fig. 9) against the irradiation distributions of several villages. These villages are located in the plains and at the same latitude as the ski resorts, but at different longitudes. All of these villages can be seen in Fig. 2 as they form two 'lines' at iso-latitude, while only four of them have been displayed in Fig. 9 for the sake of clarity.

The distribution of the mountain village is the lowest in both cases. The mountain village of Tignes has a distribution much more shifted towards low irradiations compared to its plain villages than Le Grand-Bornand. The difference of typology of this two mountain villages could partly explain the variability in the shift. Indeed, Le Grand Bornand is situated in a mountain range with lower elevation compared to the mountain range housing Tignes, resulting in reduced shading effects. Valley morphology can also be a contributing factor, with a more open valley and more distant mountains, leading to less obstruction for buildings in Le Grand-Bornand.

4.7. Influencing parameters

In order to better understand and explain the shape of the distributions and the differences observed with plain villages, the impact of topography and mountainous climate has been investigated. To that aim, for each village, two physical indicators are defined. The first indicator is the averaged Sky View Index (*SVI*) defined as:

$$SVI = \frac{1}{N_b}\sum_{i=1}^{N_b}\left(\frac{\text{Visible sky area from building i}}{\text{Unobstructed visible sky area}}\right), \quad (6)$$

with N_b the number of buildings in the investigated village.

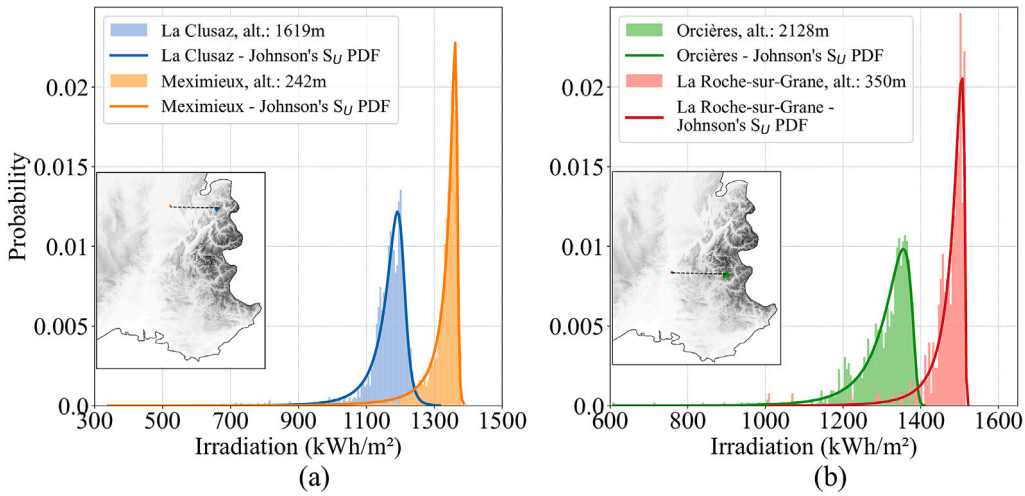

Fig. 7. Comparison of distributions of average annual irradiation on building rooftops with Johnson's S_U distribution estimation between a mountain village and a plain village at same latitude (a) in the northern Alps (La Clusaz and Meximieux (lat.: 45.904°)) and (b) in the southern Alps (Orcières and La Roche-sur-Grane (lat.: 44.683°)). A magnified view of the topographic map of France with the location of each pair of villages is also displayed. (For interpretation of the references to color in this figure legend, the reader is referred to the web version of this article.)

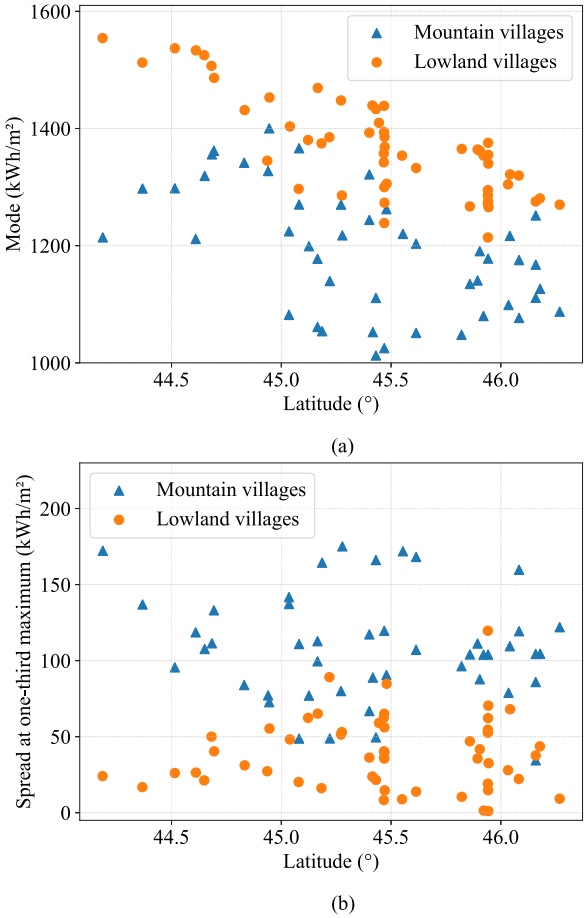

Fig. 8. Comparison of (a) the mode and (b) the spread at one-third maximum of the average annual irradiation on building rooftop distributions for mountain and lowland villages. Mountain villages are represented by blue triangles and lowland villages by orange circles.

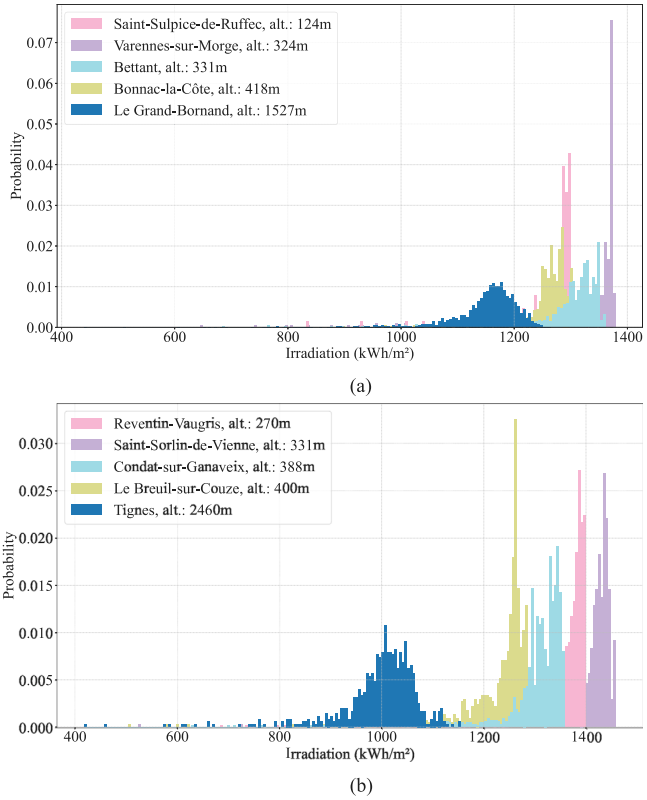

Fig. 9. Distributions of average annual irradiation on building rooftops for some villages at the same latitude as (a) Le Grand-Bornand (lat.: 45.942°) and (b) Tignes (lat.: 45.469°). (For interpretation of the references to color in this figure legend, the reader is referred to the web version of this article.)

SVI, illustrated on Fig. 10, is the averaged proportion of sky visible from village's buildings, calculated by the ratio of orange area to blue area. This indicator is inspired by the Sky View Factor [72], but only far masks are considered in the present case. It is calculated for all the buildings in each village, and the average value per village is

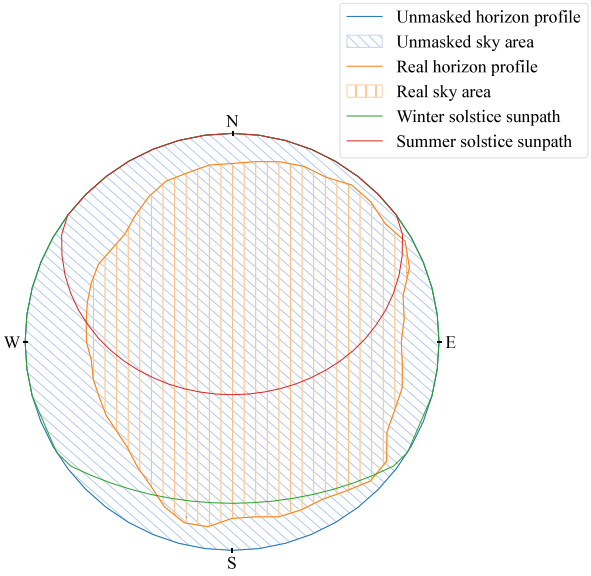

Fig. 10. Horizon profile and sky areas for the town hall of the village of Châtel. (For interpretation of the references to color in this figure legend, the reader is referred to the web version of this article.)

retained. *SVI* represents here the averaged masks due to mountains, which are impacting building rooftops. A low *SVI* indicates that the village's buildings suffer from far masks caused by mountains.

Sky areas are obtained using the *PVGIS* API [73], which provides horizon profiles. These horizon profiles take into account all the terrain features that can block sunlight at certain times of the day. They are calculated using ground elevation data with a resolution of 3 arc-seconds (around 90 m).

The second indicator, elaborated for this study, is the Diffuse Fraction Index (*DFI*). It aims at quantifying the impact of the cloud coverage and is defined as :

$$DFI = \frac{1}{N_t}\sum_{t=1}^{N_t}\left(\frac{\sum_{j=1}^{365}\left(\sum_{h=10}^{15} DHI(h,j,t)\right)}{\sum_{j=1}^{365}\left(\sum_{h=10}^{15} GHI(h,j,t)\right)}\right), \tag{7}$$

with N_t the number of tiles of the investigated village.

The ratio of the annual cumulative Diffuse Horizontal Irradiance (DHI) by the annual cumulative Global Horizontal Irradiance (GHI) is used to calculate *DFI*. *DFI* allows taking into account the cloud cover, as it will be higher if the proportion of diffuse radiation is more important. Indeed, the diffuse radiation represent the part of the global radiation that is absorbed and then reflected by clouds and particles in the atmosphere. Only hours between 10:00 and 15:00 (10 a.m. to 3 p.m.) of each day of the year are considered in the calculation. The chosen interval avoids considering far masks, as the sun is high enough in the sky at these times. Shading by surrounding terrain is already taken into account in the calculation of *SVI*. *DFI* is calculated for each meteorological file used in simulations, i.e. for each tile as presented in Section 2.3. It is then averaged for each village.

The relation between the mode and the spread at one-third maximum of the studied villages have been plotted against *SVI* and against *DFI* on Fig. 11. Linear regressions were obtained and plotted on these graphs. The coefficient of determination, R^2, which assesses the quality of the regression, was calculated and is also displayed.

It can be seen from (Fig. 11a) that the mode i.e. the cumulative energy received by the majority of roofs, increases with the *SVI*. This shows the influence that the masks have on the irradiation distribution within a mountain village. The higher the mask, the lower the energy being received by building rooftops. It is also interesting to see the impact of the latitude here. On top of the linear trend with the *SVI*, there is a secondary trend with the latitude which was already observed in Fig. 8. Incorporating the latitude in a two-variable regression model improves the R^2 up to 0.73.

Mode's value decreases linearly with the *DFI* (Fig. 11b), which is a direct consequence of a higher cloud coverage in mountainous areas. In these regions, the Foehn effect [74], which induces an increased presence of clouds on windward ascending slopes, partly explains the high cloud coverage. The variations with the latitude are not as pronounced, but lower latitudes appear to have smaller *DFI* values.

Consequently, the presence of far masks and high cloud coverages explains the shift of the distributions of rooftop irradiation observed between plains and mountains in Fig. 7.

The effects are opposite when it comes to the spread at one-third maximum. The spread increases as the *SVI* decreases, which is associated with the numerous far masks present in mountainous villages (Fig. 11c). Buildings in these villages are scattered across large territories, often spanning several mountainsides. Consequently, the terrain also contributes to the heterogeneity of incoming radiation blocked by far masks and to the variability of shading by the surrounding topography, that are added to the overshadowing effects from nearby buildings. Therefore, the irradiation received by rooftops vary significantly among buildings in mountainous areas, explaining the higher values of spread compared to plain areas (Fig. 7).

Regarding the relation between the *DFI* and the spread, no clear trends can be observed. This is mostly due to the fact that the *DFI* indicates the predominance of diffuse radiation over each village. However, these diffuse radiations generally exerts a global impact on the entire village. It thus displaces the irradiation received on all buildings, as depicted in Fig. 11b, but it affects the village uniformly and, therefore, does not contribute to the spreading of the distribution of irradiation within the village.

Hence, the mode is primarily explained by the proportion of diffuse irradiance, which determines the highest possible irradiation value for the village, while the dispersion of values is more significantly influenced by the presence of topography.

4.8. Predictions of irradiation distributions

As correlation appeared between mode, spread at one-third maximum, and the three parameters mentioned above (*SVI*, *DFI* and latitude), a prediction of the distributions has been done only by calculating these indicators. To this aim, the shape of the distributions was estimated with the prediction of fitting parameters of the Johnson's S_U distribution a, b, c, d (see Eq. (3)). The prediction of the parameters was carried out using a multiple linear regression model available in the *scikit-learn* library [75]. The model utilizes the ordinary least squares method to minimize the residual sum of squares between the observed values and the values predicted by the linear approximation.

The data obtained earlier during the simulation of villages were split into two groups, 80% for training, and 20% for testing. A linear regression model was created for each of the four parameters, with the three influencing parameters as variables.

The similarity between the Johnson's S_U function obtained through fitting with real data and the one obtained through linear regression using only the three indicators is illustrated in Fig. 12. The similarity depends on the villages but is rather promising. The quality of the prediction is assessed with the coefficient of determination R^2, as it was done for approximation by Johnson's S_U (see 4.3), calculated between raw data and the predicted distribution.

For the village of Morzine (Fig. 12a), the predicted curve closely matches the fitted one. For the village of Saint-Lager-Bressac (Fig. 12b), the result is slightly less accurate, but the predicted mode is still close to the actual mode, with only a difference in peak height. In the case of the village of Les Orres (Fig. 12c), the predicted curve deviates from the

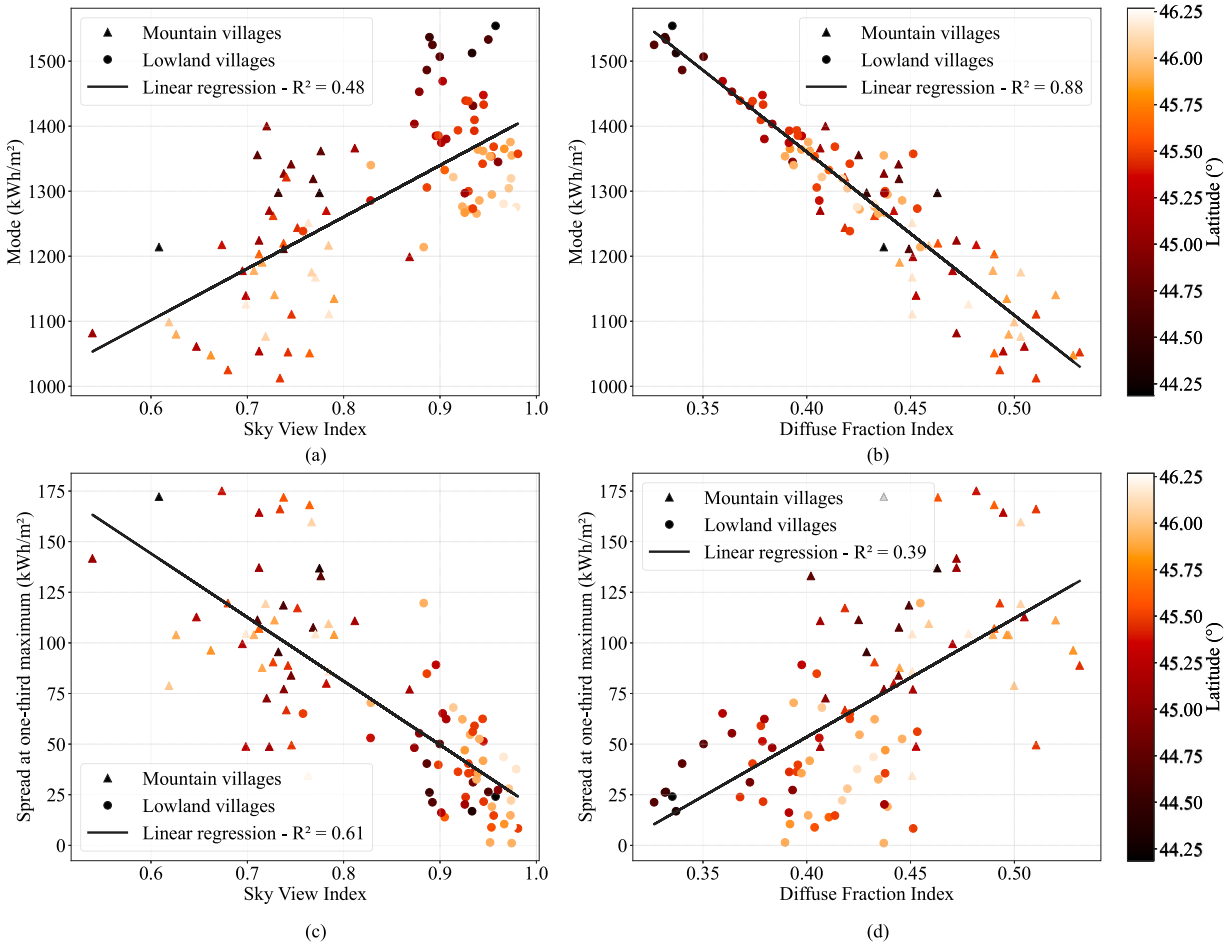

Fig. 11. At the top, relation between mode, latitude and (a) Sky View Index or (b) Diffuse Fraction Index. At the bottom, relation between spread at one-third maximum, latitude and (c) Sky View Index (*SVI*) and (d) Diffuse Fraction Index (*DFI*). Triangles represent mountain villages whereas circles represent plain villages. Each village is also colored based on its latitude, a darker color meaning a lower latitude. (For interpretation of the references to color in this figure legend, the reader is referred to the web version of this article.)

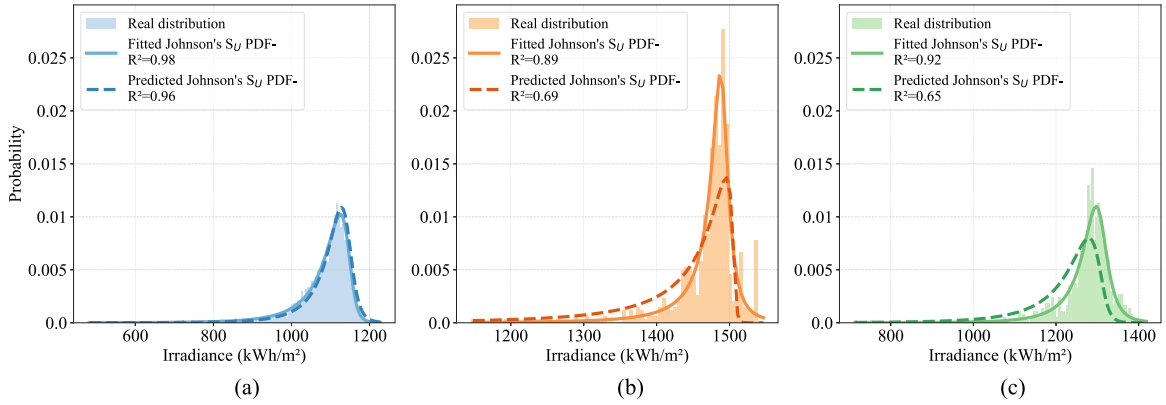

Fig. 12. Comparison of fitted Johnson's S_U PDF function and predicted for the village of (a) Morzine (lat.: 46.179°, long.: 6.709°, alt.: 1549 m), (b) Saint-Lager-Bressac (lat.: 44.694°, long.: 4.709°, alt.: 236 m) and (c) Les Orres (lat.: 44.515°, long.: 6.549°, alt.:2116 m).

fitted one, with a shift towards lower irradiation values in the obtained distribution. However, the prediction still provides useful estimates of the distributions.

To evaluate the precision of the model, the relative error between the fitted values and the predicted values of modes and spreads at one-third maximum have been calculated on the testing set. The model demonstrates good precision in predicting the mode values, with an average difference of only 2.2% and a median value of 1.5%. However, the dispersion of annual cumulative irradiation is less accurately predicted: though the median value of the relative error of the spread

is 25%, a small number of poor predictions contributes to a mean value of 76%.

The model could be probably improved to increase accuracy for all villages, but it currently offers a rapid estimation of distributions with the calculation of these indicators, without the need to run time-consuming simulations. The estimation of individual rooftop irradiation is however not possible with this model, and would require more indicators [76] or a more complex method [77].

5. Discussions and perspectives

5.1. Perspectives and impact on energy transition planning

The methodology developed in this article is valuable for assessing the solar potential of villages, especially those in mountainous regions, using publicly available databases that cover a large territory. The aim of this methodology was to be deployable on a large scale with reasonable computational time. This study has demonstrated that the distribution of rooftop irradiation in a village can be effectively characterized by an analytical function. It has been used to compare the difference of annual solar irradiation between plain and mountain villages. Furthermore, the use of latitude and two new indicators defined in this study provide an estimation of the distribution at low computational cost and an initial insight of the received irradiation.

The methodology requires a minimal amount of data and offers significant flexibility, thanks to the use of *QGIS* software and *Python* extensions. As a result, it can be applied to villages located in various regions or countries to conduct similar studies or simply to generate a solar cadastre for identifying sunny rooftops.

Solar cadastres and distributions of irradiation within a village, along with their predictions, can be valuable for energy planning purposes at the scale of one or multiple villages. Indeed, to deploy a solar strategy in mountainous areas, it is crucial in a first time to evaluate solar resources in these territories. The distribution of solar irradiation over the mountainous territories needs to be understood, as it differs from the distribution of plain villages. With the high number of mountain villages analyzed in this study, it is possible to have a broad overview of the distribution of solar energy in mountainous municipalities and observe several cases.

The first conclusion that could be drawn is that, despite the presence of shading and cloud cover, solar resources remain sufficiently high in mountainous areas to be of interest. Indeed, buildings' rooftops or ground surfaces could receive a cumulative annual irradiation between 1300 and 1400 kWh/m^2 in almost all the villages. Therefore, these villages should not be neglected in energy transition planning.

Secondly, this study reveals that the morphology of mountain villages – in particular building's location – can lead to significant variations in rooftop potentials. The main trend is a higher dispersion (spread at one-third maximum) than in plains due to far masks shading. Moreover, for certain villages, distinct zones of irradiation may emerge as explained in Section 4.4. This second result shows that geographical boundaries define building clusters that do not necessarily match with administrative boundaries. This information could be of importance for local decision makers to select areas of interest (i.e. high irradiation zones).

The benefits of utilizing available solar energy could be higher in mountains than in flat terrain, as mountain villages are isolated and have high energy demands, especially in winter. Solar maps could be utilized by decision-makers within municipalities to gain a better understanding of the potential of renewable energy generation and, consequently, the potential for energy self-sufficiency.

Lastly, further development of a model to estimate photovoltaic or thermal production could be beneficial. This would enable to estimate the amount of electricity and heat that could be produced by each village or "irradiation sub-village". To that aim, an accurate modeling of the impact of snow on PV and thermal systems would be required. This would be valuable information for the promotion of the development of solar systems in mountain villages.

5.2. Uncertainties

Many sources of uncertainty are present in our study. These sources primarily stem from the inputs of our model. Firstly, the meteorological data required to estimate the annual cumulative irradiation from SEBE is the largest source of uncertainty. Indeed, this data is estimated from satellite models with a resolution of only 5 km × 5 km. Despite the overall good accuracy of these data, precision may degrade in mountainous areas due to the presence of snow, which can be confused by algorithms with cloud cover. Furthermore, geographic data such as the DTM and cadastral data also contain uncertainties. The spatial resampling of the DTM, from 25 m resolution to a resolution compatible with building scale, adds to uncertainties. Cadastral data are also simplified representations of building shapes. Subsequently, the SEBE tool contains several sources of uncertainty, which may arise from the patch redistribution model or the Reindl model [62] for estimating the diffuse component.

Thus, irradiation received by buildings entail numerous uncertainties, but the probabilistic approach used with distribution analysis and the use of the mode to describe irradiation received by villages help smooth the uncertainties associated with the deterministic approach of the SEBE tool.

5.3. Limitations

One limitation of this study is the impossibility to accurately account for the real structure and the morphology of rooftops due to a lack of data, particularly the consideration of orientations and slopes. It would have been possible to define standardized orientations and slopes based on typical French roof morphologies. But dwellings located in mountain area often have unique roof structures. For instance, it is common to find roofs with two slopes oriented along the width of the buildings, rather than the length, as is more typical in the rest of the country. More generally, the diversity of rooftops within a given territory makes it challenging to use average values. However, when more accurate data will become available, such as precise LiDAR data (LIght Detection and Ranging), the consideration of orientation and slope will be feasible using this methodology.

In this study, about a hundred villages were selected with the aim of observing the difference between lowland and mountainous areas. It would also be interesting to study villages across the entire French territory, which could not been possible so far due to the computational time required by the simulations. Indeed, the simulation durations were relatively long and roughly proportional to the size of the municipalities. The total duration of the simulation, including data preprocessing and postprocessing, for a village of average area (40 km^2) is approximately 12 h and exceeded 5 days for the largest village. The machine we used to run simulations is a shared working station. It is equipped with an Intel Xeon W-2125 CPU (release date Q3 2017) and 256 GB of memory. It runs Ubuntu 22.04. An Anaconda environment with the following packages and plugins was used: Python (3.9.17), Qgis (3.32.2), GDAL (3.7.1), UMEP for processing (2.0.1). No computation was done on GPU due to a software limitation, yet it could largely speed up some of the processing steps.

6. Conclusion

A methodology was developed in order to adapt existing tools for irradiation prediction on buildings to large mountainous territories. This approach employs a DSM combined with a tiling methodology to consider distant obstructions, thus accounting for the terrain. This methodology is entirely based on open-access data sources (IGN, EU-DEM) and on existing open-source algorithms (QGIS, SEBE). Rooftop irradiation for 92 municipalities, located in both mountainous and plain areas is calculated. The distributions of the irradiation on building rooftops are observed to follow a similar pattern that can be

well approximated by a continuous probability distribution, here a Johnson's S_U distribution function. Exceptions are observed in certain mountainous villages, which could be addressed through the clustering of buildings based on their locations and fitting the distribution function to each cluster accordingly. This approximation facilitated the characterization of distributions using multiple indicators and the analysis of distributions disparities between plain and mountain villages. Distributions are shifted towards lower irradiations and show greater dispersions for mountain villages. Two indicators, the Sky View Index and the Diffuse Fraction Index, were defined to explain the observed differences. The presence of mountainous terrain and cloud cover were thus identified as factors contributing to reduced solar radiation in mountainous regions. The presence of far masks and of specific village morphologies in mountainous areas also leads to higher variability in irradiation values within a village compared to plain villages. Through a multiple linear regression model, the density function could be predicted using the two aforementioned indicators and the latitude as variables. Despite varying results across the studied villages, this model enables obtaining preliminary outcomes with reduced computational times.

This study has thereby highlighted that the characteristics of mountainous regions have a significant impact on solar potential. These conclusions could be used to establish energy planning strategies for mountainous areas, with the solar cadastres here obtained helping to determine the priority areas for installations of rooftop solar systems.

Declaration of competing interest

The authors declare that they have no known competing financial interests or personal relationships that could have appeared to influence the work reported in this paper.

Data availability

The workflow developed in this article is published open-source on GitHub as a tool named *toscana* (https://github.com/locie/toscana.git).

Acknowledgments

This work have been supported by European University UNITA, the Grand [La]Bo project, CITEE French swiss Chair and by the French National Research Agency, through the Investments for Future Program (ref. ANR-18-EURE-0016 - Solar Academy). The research units LOCIE and LISTIC are members of the INES Solar Academy Research Center.

References

[1] LOI n° 2023-175 du 10 mars 2023 relative à l'accélération de la production d'énergies renouvelables, J. Off. (2023).
[2] A. Polderman, A. Haller, D. Viesi, X. Tabin, S. Sala, A. Giorgi, L. Darmayan, J. Rager, J. Vidovič, Q. Daragon, et al., How can ski resorts get smart? Transdisciplinary approaches to sustainable winter tourism in the European Alps, Sustainability 12 (14) (2020) 5593.
[3] N.M. Katsoulakos, D.C. Kaliampakos, What is the impact of altitude on energy demand? A step towards developing specialized energy policy for mountainous areas, Energy Policy 71 (2014) 130–138.
[4] E.B. Weiss, United nations conference on environment and development, Int. Legal Mater. 31 (4) (1992) 814–817.
[5] U.N.G. Assembly, Sustainable mountain development, 2013.
[6] D. Greenland, in: J.E. Oliver, R.W. Fairbridge (Eds.), Mountain Climates, Upland. The Encyclopedia of Climatology, Van Nostrand Reinhold, New York, 1987.
[7] H. Liniger, R. Weingartner, Mountains and freshwater supply, Unasylva 49 (195) (1998) 39–46.
[8] N. Katsoulakos, Optimal Use of Renewable Energy Sources in Mountainous Areas. The Case of Metsovo, Greece (Ph.D. thesis, Doctoral thesis), National Technical University of Athens, School of Mining, 2013.
[9] N.M. Katsoulakos, D.C. Kaliampakos, The energy identity of mountainous areas: the example of Greece, J. Mountain Sci. 15 (7) (2018) 1429–1445.
[10] P. Vuichard, A. Stauch, R. Wüstenhagen, Keep it local and low-key: Social acceptance of alpine solar power projects, Renew. Sustain. Energy Rev. 138 (2021) 110516.
[11] P. Díaz, O. van Vliet, Drivers and risks for renewable energy developments in mountain regions: a case of a pilot photovoltaic project in the Swiss Alps, Energy Sustain. Soc. 8 (2018) 1–17.
[12] H. François, R. Samacoïts, D.N. Bird, J. Köberl, F. Prettenthaler, S. Morin, Climate change exacerbates snow-water-energy challenges for European ski tourism, Nature Clim. Change (2023) 1–8.
[13] J. Polo, R.J. García, Solar potential uncertainty in building rooftops as a function of digital surface model accuracy, Remote Sens. 15 (3) (2023) 567.
[14] A.A.A. Gassar, S.H. Cha, Review of geographic information systems-based rooftop solar photovoltaic potential estimation approaches at urban scales, Appl. Energy 291 (2021) 116817.
[15] J. Kanters, M. Wall, E. Kjellsson, The solar map as a knowledge base for solar energy use, Energy Procedia 48 (2014) 1597–1606, http://dx.doi.org/10.1016/j.egypro.2014.02.180.
[16] G. Li, Z. Wang, C. Xu, T. Li, J. Gao, Q. Mao, S. Chen, A district-scale spatial distribution evaluation method of rooftop solar energy potential based on deep learning, Sol. Energy 268 (2024) 112282.
[17] F. Hasti, J. Mamkhezri, R. McFerrin, N. Pezhooli, Optimal solar photovoltaic site selection using geographic information system–based modeling techniques and assessing environmental and economic impacts: The case of Kurdistan, Sol. Energy 262 (2023) 111807.
[18] F.C. Jong, M.M. Ahmed, Novel GIS-based fuzzy TOPSIS and filtration algorithms for extra-large scale optimal solar energy sites identification, Sol. Energy 268 (2024) 112274.
[19] L. Laiti, D. Andreis, F. Zottele, L. Giovannini, L. Panziera, G. Toller, D. Zardi, A solar atlas for the Trentino region in the Alps: quality control of surface radiation data, Energy Procedia 59 (2014) 336–343.
[20] F. Nex, F. Remondino, G. Agugiaro, R. De Flippi, M. Poletti, C. Furlanello, S. Menegon, G. Dallago, S. Fontanari, 3D solarweb: A solar cadaster in the Italian alpine landscape, Int. Arch. Photogram. Remote Sens. Spat. Inf. Sci. 40 (2013) 173–178.
[21] M. Šúri, J. Hofierka, A new GIS-based solar radiation model and its application to photovoltaic assessments, Trans. GIS 8 (2) (2004) 175–190.
[22] M. Liu, A. Bárdossy, J. Li, Y. Jiang, GIS-based modelling of topography-induced solar radiation variability in complex terrain for data sparse region, Int. J. Geogr. Inf. Sci. 26 (7) (2012) 1281–1308.
[23] S. Zhang, X. Li, J. She, X. Peng, Assimilating remote sensing data into GIS-based all sky solar radiation modeling for mountain terrain, Remote Sens. Environ. 231 (2019) 111239.
[24] R. Dubayah, P.M. Rich, Topographic solar radiation models for GIS, Int. J. Geogr. Inf. Syst. 9 (4) (1995) 405–419.
[25] X. Pons, M. Ninyerola, Mapping a topographic global solar radiation model implemented in a GIS and refined with ground data, Int. J. Climatol.: J. R. Meteorol. Soc. 28 (13) (2008) 1821–1834.
[26] M. Olson, S. Rupper, Impacts of topographic shading on direct solar radiation for valley glaciers in complex topography, Cryosphere 13 (1) (2019) 29–40.
[27] S.Y. Alsadi, Y.F. Nassar, A general expression for the shadow geometry for fixed mode horizontal, step-like structure and inclined solar fields, Sol. Energy 181 (2019) 53–69.
[28] A. Carpentieri, D. Folini, M. Wild, L. Vuilleumier, A. Meyer, Satellite-derived solar radiation for intra-hour and intra-day applications: Biases and uncertainties by season and altitude, Sol. Energy 255 (2023) 274–284.
[29] J.A. Olseth, A. Skartveit, Spatial distribution of photosynthetically active radiation over complex topography, Agricult. Forest Meteorol. 86 (3–4) (1997) 205–214.
[30] P.E. Thornton, S.W. Running, M.A. White, Generating surfaces of daily meteorological variables over large regions of complex terrain, J. Hydrol. 190 (3–4) (1997) 214–251.
[31] X.-F. QIU, Y. ZENG, S.-M. LIU, Distributed modeling of extraterrestrial solar radiation over rugged terrain, Chin. J. Geophys. 48 (5) (2005) 1100–1107.
[32] W.A. Hetrick, P.M. Rich, F.J. Barnes, S.B. Weiss, GIS-based solar radiation flux models, in: ACSM ASPRS Annual Convention, Vol.3, AMERICAN SOC PHOTOGRAMMETRY & REMOTE SENSING+ AMER CONG ON, 1993, 132–132.
[33] L. Kumar, A.K. Skidmore, E. Knowles, Modelling topographic variation in solar radiation in a gis environment, Int. J. Geogr. Inf. Sci. 11 (5) (1997) 475–497.
[34] I. Mészároš, Modelovanie príkonu slnečnej energie na horské povodie, Acta Hydrol. Slovaca 1 (1998) (1998) 68–75.
[35] P. Miklánek, The estimation of energy income in grid points over the basin using simple digital elevation model, in: Annales Geophysicae, vol. 11, 11 European Geophysical Society, Springer, 1993, pp. 296–312.
[36] J.P. Wilson, J.C. Gallant, Terrain Analysis: Principles and Applications, John Wiley & Sons, 2000.
[37] P. Fu, P.M. Rich, Design and implementation of the solar analyst: an ArcView extension for modeling solar radiation at landscape scales, in: Proceedings of the Nineteenth Annual ESRI User Conference, Vol. 1, San Diego USA, 1999, pp. 1–31.
[38] J. Tovar-Pescador, D. Pozo-Vázquez, J. Ruiz-Arias, J. Batlles, G. López, J. Bosch, On the use of the digital elevation model to estimate the solar radiation in areas of complex topography, Meteorol. Appl. 13 (3) (2006) 279–287.

[39] G. Lopez, F.J. Batlles, J. Tovar-Pescador, A new simple parameterization of daily clear-sky global solar radiation including horizon effects, Energy Convers. Manage. 48 (1) (2007) 226–233.
[40] G. López, F.J. Batlles, Estimating solar radiation from MODIS data, Energy Procedia 49 (2014) 2362–2369.
[41] J. Bosch, F. Batlles, L. Zarzalejo, G. López, Solar resources estimation combining digital terrain models and satellite images techniques, Renew. Energy 35 (12) (2010) 2853–2861.
[42] J.-K. Park, A. Das, J.-H. Park, A new approach to estimate the spatial distribution of solar radiation using topographic factor and sunshine duration in South Korea, Energy Convers. Manage. 101 (2015) 30–39.
[43] O. Antonić, J. Križan, A. Marki, D. Bukovec, Spatio-temporal interpolation of climatic variables over large region of complex terrain using neural networks, Ecol. Model. 138 (1–3) (2001) 255–263.
[44] J. Bosch, G. Lopez, F. Batlles, Daily solar irradiation estimation over a mountainous area using artificial neural networks, Renew. Energy 33 (7) (2008) 1622–1628.
[45] J. Heo, J. Jung, B. Kim, S. Han, Digital elevation model-based convolutional neural network modeling for searching of high solar energy regions, Appl. Energy 262 (2020) 114588.
[46] N. Mohajeri, A. Perera, S. Coccolo, L. Mosca, M. Le Guen, J.-L. Scartezzini, Integrating urban form and distributed energy systems: Assessment of sustainable development scenarios for a Swiss village to 2050, Renew. Energy 143 (2019) 810–826.
[47] M. Le Guen, L. Mosca, A.T.D. Perera, S. Coccolo, N. Mohajeri, J.-L. Scartezzini, Improving the energy sustainability of a Swiss village through building renovation and renewable energy integration, Energy Build. 158 (2018) 906–923.
[48] D. Assouline, N. Mohajeri, J.-L. Scartezzini, Quantifying rooftop photovoltaic solar energy potential: A machine learning approach, Sol. Energy 141 (2017) 278–296.
[49] G. Mavromatidis, K. Orehounig, J. Carmeliet, Evaluation of solar energy integration potential in a neighborhood, in: Proceedings of BS2015, Hyderabad, India, Dec, 2015, pp. 7–9.
[50] K. Orehounig, R. Evins, V. Dorer, Integration of decentralized energy systems in neighbourhoods using the energy hub approach, Appl. Energy 154 (2015) 277–289.
[51] D. Notzon, P. Florio, A. Schüler, Solar energy potential at the great st bernard pass, in: Journal of Physics: Conference Series, Vol. 2042, IOP Publishing, 2021, 012104.
[52] R. Pueblas, P. Kuckertz, J.M. Weinand, L. Kotzur, D. Stolten, ETHOS. PASSION: An open-source workflow for rooftop photovoltaic potential assessments from satellite imagery, Sol. Energy 265 (2023) 112094.
[53] INSEE, Code officiel géographique, 2023, URL: https://www.insee.fr/fr/metadonnees/source/serie/s2084. (Consulted 12 September 2023).
[54] GDAL/OGR contributors, GDAL/OGR Geospatial Data Abstraction software Library, Open Source Geospatial Foundation, 2023, http://dx.doi.org/10.5281/zenodo.5884351, URL: https://gdal.org.
[55] T. Huld, R. Müller, A. Gambardella, A new solar radiation database for estimating PV performance in Europe and Africa, Sol. Energy 86 (6) (2012) 1803–1815, http://dx.doi.org/10.1016/j.solener.2012.03.006, URL: https://www.sciencedirect.com/science/article/pii/S0038092X12001119.
[56] F. Lindberg, P. Jonsson, T. Honjo, D. Wästberg, Solar energy on building envelopes–3D modelling in a 2D environment, Sol. Energy 115 (2015) 369–378.
[57] European Environment Agency, EU-DEM, 2023, URL: https://land.copernicus.eu/imagery-in-situ/eu-dem. (Consulted 12 September 2023).
[58] IGN, BD TOPO®, 2023, URL: https://geoservices.ign.fr/bdtopo. (Consulted 12 September 2023).
[59] A.R. Jensen, K.S. Anderson, W.F. Holmgren, M.A. Mikofski, C.W. Hansen, L.J. Boeman, R. Loonen, pvlib iotools—Open-source python functions for seamless access to solar irradiance data, Sol. Energy 266 (2023) 112092.
[60] R. Urraca, A.M. Gracia-Amillo, E. Koubli, T. Huld, J. Trentmann, A. Riihelä, A.V. Lindfors, D. Palmer, R. Gottschalg, F. Antonanzas-Torres, Extensive validation of CM SAF surface radiation products over Europe, Remote Sens. Environ. 199 (2017) 171–186.
[61] C. Ratti, P. Richens, Urban texture analysis with image processing techniques, in: Computers in Building: Proceedings of the CAADfutures'99 Conference. Proceedings of the Eighth International Conference on Computer Aided Architectural Design Futures Held At Georgia Institute of Technology, Atlanta, Georgia, USA on June 7–8, 1999, Springer, 1999, pp. 49–64.
[62] D.T. Reindl, W.A. Beckman, J.A. Duffie, Diffuse fraction correlations, Solar Energy 45 (1) (1990) 1–7.
[63] P. Tregenza, Daylighting algorithms, 1993.
[64] G. Desthieux, C. Carneiro, R. Camponovo, P. Ineichen, E. Morello, A. Boulmier, N. Abdennadher, S. Dervey, C. Ellert, Solar energy potential assessment on rooftops and facades in large built environments based on lidar data, image processing, and cloud computing. methodological background, application, and validation in geneva (solar cadaster), Front. Built Environ. (2018) 14.
[65] R.S. Carson, Alternatives for managing atmospheric warming, in: INCOSE International Symposium, Vol. 29, Wiley Online Library, 2019, pp. 937–951.
[66] A.H. Duhis, M. Aljanabi, M.S.S. Al-Kafaji, Increasing photovoltaic system power output with white paint albedo–a scenario in Al-Mausaib city using PVSyst. software, Int. J. Power Electron. Drive Syst. (IJPEDS) 14 (2) (2023) 1149–1159.
[67] R.E. Pawluk, Y. Chen, Y. She, Photovoltaic electricity generation loss due to snow–A literature review on influence factors, estimation, and mitigation, Renew. Sustain. Energy Rev. 107 (2019) 171–182.
[68] The SciPy community, Statistical functions (scipy.stats), 2023, URL: https://docs.scipy.org/doc/scipy/reference/stats.html. (Consulted 12 September 2023).
[69] N.L. Johnson, Systems of frequency curves generated by methods of translation, Biometrika 36 (1/2) (1949) 149–176.
[70] H.-S. Park, C.-H. Jun, A simple and fast algorithm for K-medoids clustering, Expert Syst. Appl. 36 (2) (2009) 3336–3341.
[71] G. Kopp, Daily solar flux as a function of latitude and time, Sol. Energy 249 (2023) 250–254.
[72] M. Dirksen, R. Ronda, N. Theeuwes, G. Pagani, Sky view factor calculations and its application in urban heat island studies, Urban Clim. 30 (2019) 100498.
[73] Joint Research Centre, Horizon profile, 2023, URL: https://joint-research-centre.ec.europa.eu/photovoltaic-geographical-information-system-pvgis/pvgis-tools/horizon-profile_en. (Consulted 12 September 2023).
[74] H. Richner, P. Hächler, Understanding and forecasting alpine foehn, in: Mountain Weather Research and Forecasting: Recent Progress and Current Challenges, Springer, 2013, pp. 219–260.
[75] F. Pedregosa, G. Varoquaux, A. Gramfort, V. Michel, B. Thirion, O. Grisel, M. Blondel, P. Prettenhofer, R. Weiss, V. Dubourg, J. Vanderplas, A. Passos, D. Cournapeau, M. Brucher, M. Perrot, E. Duchesnay, Scikit-learn: Machine learning in python, J. Mach. Learn. Res. 12 (2011) 2825–2830.
[76] A. Boccalatte, M. Thebault, C. Ménézo, J. Ramousse, M. Fossa, Evaluating the impact of urban morphology on rooftop solar radiation: A new city-scale approach based on Geneva GIS data, Energy Build. 260 (2022) 111919.
[77] A. Walch, R. Castello, N. Mohajeri, J.-L. Scartezzini, Big data mining for the estimation of hourly rooftop photovoltaic potential and its uncertainty, Appl. Energy 262 (2020) 114404.